MNE 16 (2022) 100149

Contents lists available at ScienceDirect

Micro and Nano Engineering

journal homepage: www.sciencedirect.com/journal/micro-and-nano-engineering

Label-free multi-step microfluidic device for mechanical characterization of blood cells: Diabetes type II

Diana Pinho [a,b,1,*], Vera Faustino [c,d,e], Susana O. Catarino [c,d], Ana I. Pereira [a], Graça Minas [c,d], Fernando T. Pinho [b,f], Rui Lima [e]

[a] Research Centre in Digitalization and Intelligent Robotics (CeDRI), Instituto Politécnico de Bragança, Campus de Santa Apolónia, 5300-253 Bragança, Portugal
[b] CEFT, Faculdade de Engenharia da Universidade do Porto (FEUP), Rua Roberto Frias, 4200-465 Porto, Portugal
[c] Center for MicroElectromechanical Systems (CMEMS-UMinho), University of Minho, Campus de Azurém, 4800-058 Guimarães, Portugal
[d] LABBELS-Associate Laboratory, Braga/Guimarães, Portugal
[e] MEtRICs, Mechanical Engineering Department, University of Minho, Campus de Azurém, 4800-058 Guimarães, Portugal
[f] ALiCE, Faculdade de Engenharia da Universidade do Porto (FEUP), Rua Roberto Frias, 4200-465 Porto, Portugal

ARTICLE INFO

Keywords:
Hydrodynamic separation
Blood-on-a-chip
Viscosity
Deformability
Diabetes type II
Biomicrofluidics

ABSTRACT

The increasing interest to establish significant correlations between blood cell mechanical measurements and blood diseases, has led to the promotion of microfluidic devices as attractive clinical tools for potential use in diagnosis. A multi-step microfluidic device able to separate red and white blood cells (RBCs and WBCs) from plasma and simultaneously measure blood cells deformability (5 and 20% of hematocrit) is presented in this paper. The device employs passive separation based on the cross-flow filtration principle, introduced at each daughter channel. At the outlets, hyperbolic geometries allow single-cell deformability analysis. The device was tested with blood from five healthy and fifteen diabetic type II voluntary donors. The results have shown that WBCs have lower deformability than RBCs, and no significant differences were observed in WBCs from healthy and pathological blood samples. In contrast, RBCs have shown significant differences, with pathological cells exhibiting lower deformability. Shear rheology has shown that blood from patients with type II diabetes has higher viscosity than blood from healthy donors. This microfluidic device has demonstrated the ability to reduce cell concentration at the outlets down to 1%, an ideal cell concentration for assessing the blood cells deformability, under healthy and pathological conditions. The results provide new insights and quantitative information about the hemodynamics of *in vitro* type II diabetes mellitus RBCs. Thus, such device can be a promising complement in clinical diagnosis and biological research as part of an integrated blood-on-a-chip system.

1. Introduction

Currently, microfluidic technologies are a powerful way to rapidly and efficiently manipulate blood samples at low cost. In particular, they allow portable and low cost *in vitro* clinical devices for efficient blood fractionation into its different components, using small volumes of samples for the diagnosis of pathologies [1–4]. The separation of red blood cells (RBCs) from plasma and the quantification of proteins, cholesterol and glucose are examples of conventional routine assays for the diagnosis and monitoring of many diseases, such as malaria, cardiovascular disease and type II diabetes mellitus [5–8].

Blood cells can be severely affected by several pathologies. For example, white blood cells (WBCs) play an important role in the immune response to allergies and infections, and contain a wealth of information about the immune status of the body [9,10]. Regarding RBCs, several biomechanical properties (*e.g.* deformability, shape, density or aggregability) are important functional biomarkers with significant potential to be applied in the biomedical and clinical research of diseases, such as diabetes, cholesterol, malaria, coronary diseases and obesity [5,8,11–14]. Additionally, by guaranteeing easy optical access to the microfluidic devices, they become powerful tools to perform direct visualizations of the cells shape and deformability with similar conditions as *in vivo* microcirculation, helping for a better understanding of the diseases' abnormal deformability behavior [6,8,13,15].

* Corresponding author at: CEFT, Faculdade de Engenharia da Universidade do Porto (FEUP), Rua Roberto Frias, 4200-465 Porto, Portugal.
E-mail address: diana.pinho@inl.int (D. Pinho).
[1] Current affiliation: International Iberian Nanotechnology Laboratory, Av. Mestre José Veiga s/n, 4715–330 Braga, Portugal.

https://doi.org/10.1016/j.mne.2022.100149
Received 18 October 2021; Received in revised form 13 April 2022; Accepted 21 May 2022
Available online 26 May 2022

Microfluidic approaches for blood cells and plasma separation can be based on passive or active separation techniques [3,16,17]. Some authors have reported efficient cell separation (95% RBCs removed from the initial whole blood [18], 99.55% of plasma separation [3]) and sorting, taking into account the size, shape, deformability and sedimentation of cells [3,18,19]. Other separation techniques are based on hemodynamic and geometrical effects, such as the existence of a cell-free layer (CFL) and the bifurcation law for hematocrit (Hct) reduction [20]. Some authors have also achieved the separation of tumor cells from healthy cells based on geometric effects [18,19,21–24]. However, regarding the sorting of WBCs and RBCs and, simultaneously, the measurement of their deformability and shape, few studies were found. Sethu et al. [25] have developed a microfluidic device based on geometric filters to separate cells by size and obtain leucocytes from whole blood, but did not measure any physical characteristics of the separated cells. Rosenbluth et al. [10] have developed a microfluidic device based on biophysical flow cytometry to measure the WBCs deformability, previously isolated from a blood sample with leukemia, using the histopaque method. Similarly, Rodrigues et al. [26] have first separated WBCs from whole blood, and then performed flow tests in a continuous pillar-type filtration microfluidic device to measure the deformation index of both WBCs and RBCs.

Diabetes mellitus type II is a disorder characterized by high blood sugar (hyperglycemia) and is commonly associated with alterations in the blood cells deformability and blood viscosity, that may cause serious microvascular complications [14,27]. Blood viscosity depends on the interaction between the molecules and cells and is proportional to the resistance to the free sliding of the blood layers within the circulation [28]. An increase of the blood viscosity can promote high blood pressure, with harmful consequences to the heart activity and walls of the vascular network. Also, following Poiseuille's law, blood viscosity is inversely proportional to flow rate and might, therefore, reduce the delivery of insulin and glucose to peripheral tissues, leading to insulin resistance and/or diabetes [28]. Most of the diabetes-focused studies performed to date in rheometers and microfluidic devices have been based on the ability of RBCs to deform [29,30] or on the increase of blood viscosity [31]. Overall, these studies have shown that the presence of a high blood glucose level contributes to disturbances of the whole blood viscosity and, in particular, to the RBCs deformability and agglomeration [32]. Fundamental rheological tests, such as steady shear flow tests [33], small and large amplitude oscillatory shear flow tests [34,35] and creep flow tests [32] have proven their relevance and can provide a better understanding and characterization of blood properties and the relation with their microstructure [15,31,33].

To go a step further, it is necessary to combine blood rheology with cells deformability measurements. Such goal is attempted here by performing, first, the rheological characterization of the fluids, specifically, steady shear viscosity tests of whole blood from healthy and type II diabetic donors. The viscous behavior of the working fluids used in the separation experiments is also evaluated. By using the developed multi-step microfluidic device, the sorting and deformability analysis of WBCs and RBCs are also performed with healthy ($n = 5$) and pathological ($n = 15$) blood samples, diluted at both 5 and 20% Hct.

2. Materials and methods

2.1. Microfluidic device design and working principle

The developed multi-step microfluidic device is a polydimethylsiloxane (PDMS) microchannel bonded to a glass substrate coated with a thin layer of PDMS. The PDMS microchannel was fabricated through replica molding, from SU-8 molds using a low-cost soft-lithography method [36], without the need for cleanroom facilities, and with ultraviolet exposure equipment [36,37]. Inlet and outlet holes were performed by using a 1.5 mm biopsy punch.

The microfluidic device comprises several stages of cross-flow filtration barriers (zones A, B and C in Fig. 1), with a 35 μm height (normal to the plane of the figure). The main channel has a length of 27.66 mm and a width of 300 μm (see Fig. 1). The cross-flow filtration takes place at various sequential pillar arrays, each made of ten rectangular pillars (50 × 55 μm) defining eleven channels of 12 μm width. These arrays are used in all levels of separation, A, B and C. The microchannel has nine outlets, eight of them preceded by four parallel sets of three hyperbolic contractions, as exhibited in zone D of Fig. 1. The hyperbolic contraction geometry has a 19 μm width at the smallest contraction size and a length of 375 μm, following the equation proposed by James et al. [38], to impose a constant strain rate along the centerline of the microchannel outlets. The multi-step microdevice has geometric symmetry relative to the main streamwise center plane (dashed line in Fig. 1), and we found the flow field to be symmetric relative to that plane. This geometry results from previous works [26,39] in which the number of pillars, gap sizes, levels of separation and downstream geometry shape was heuristically optimised, leading to the present design as the most suitable for the purpose of reducing cell concentration, from an inlet blood sample, to a minimum amount of individual cells in order to perform reliable cell deformability analysis at the outlets. This design can be further optimised especially if the objective is changed, for instance, to ensure total plasma separation or enhanced separation efficiency.

2.1.1. Cross-flow filtration and hydrodynamic effects (size, density, deformability and morphology)

By implementing a cross-flow filtration approach combined with the Zweifach-Fung effect, an efficient cell sorting along the sequential separation regions (zones A, B and C at Fig. 1) is expected. The device design takes into consideration the dimensions of the cells and the hydrodynamic effects: RBCs have a biconcave discoid shape, with a major diameter of about 8 μm and WBCs can be roughly spherical, with diameters between 8 and 20 μm [40]; in addition, WBCs present a lower density (~1090 Kg m^{-3}) than RBCs (~1100 Kg m^{-3}) [41]. For that purpose, the cross-flow region comprises an array of 11 parallel 12 μm wide channels, which promote the separation of cells with dimensions up to the gap size (12 μm). Since these channels are perpendicular to the main channel flow, the larger cells tend to flow tangentially, rather than flowing through the gaps [18,42].

2.1.2. Extensional flow and cell deformability assessment

The nine outlets were numbered from O1 to O9, as shown in Fig. 2. At each outlet, four parallel sequences of hyperbolic microchannels impose a strong extensional flow. These characteristics allow the assessment of the cells deformability. Cells moving along the centerline of the hyperbolic-shaped contractions do not suffer from other complex motions, such as rotation and tumbling [43–46]. Also, the hyperbolic micro-contraction generates a region of nearly constant strain rate and strong homogenous extensional flow away from its walls, thus constituting a promising strategy to assess single-cell deformability. It can be used as a simple and inexpensive platform suitable to detect and diagnose several diseases related to cells deformability.

2.2. Blood samples preparation

All blood samples were collected into 2.7 mL BD-vacutainer tubes. The experiments were performed with healthy ($n = 5$) and pathological ($n = 15$) human blood samples, donated from different voluntary donors. To reduce donor-to-donor variability our pathological samples were collected from patients of middle age (38–48), with a clinical follow-up of several years and with the indication that the disease was under control. Hematocrit concentrations of 5% and 20% in Dextran 40 (Dx 40) were used from healthy and pathological samples acquired from donors with a diabetes mellitus type II diagnosis, for separation and deformability assays. For the whole blood viscosity measurements, for standardization purposes, only blood samples (both healthy and

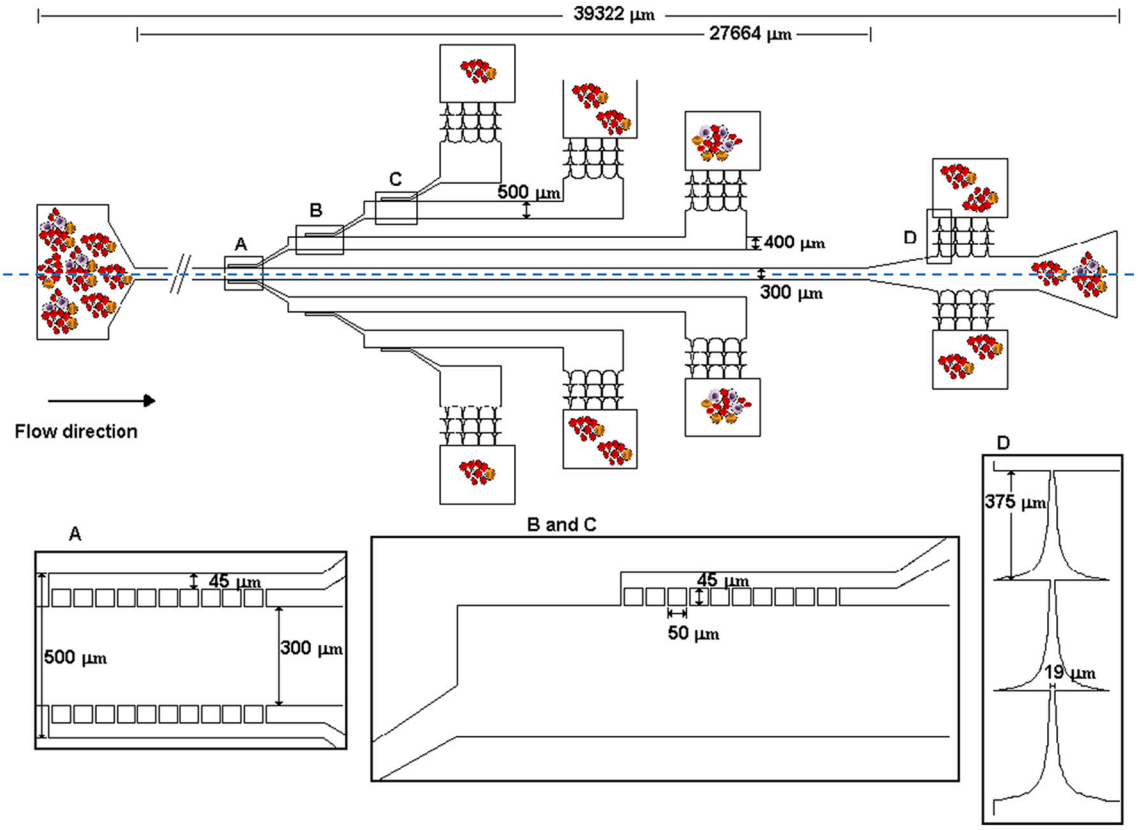

Fig. 1. Schematic view of the microchannel design and its main dimensions. Details of zones A, B, C and D. The blue dashed line represents the axis of symmetry of the multi-step microdevice. (For interpretation of the references to colour in this figure legend, the reader is referred to the web version of this article.)

pathological) with 48% Hct were prepared. Note that Dx 40 was used to reduce cells agglomeration and sedimentation during the experimental assays. All procedures were performed after patient informed consent and approval by the Ethics Committee of Bragança Hospital.

2.3. Rheometer characteristics and measurements

Sample viscosity was measured using a rotational rheometer (Bohlin CVO, Malvern, Worcestershire, UK), with a 55 mm diameter cone-plate geometry and a gap of 50 µm. Steady shear flow curves were obtained in a range of shear rates of $1 \leq \dot{\gamma}/s^{-1} \leq 10{,}000$ at temperatures of 37 °C and 22 °C, which correspond to the body temperature and *in vitro* blood experiments, respectively.

2.4. Experimental set-up

The high-speed video microscopy system used in the present study consisted of an inverted microscope (IX71, Olympus) combined with a high-speed camera (Fastcam SA5, Photron, USA), Fig. 3. The PDMS microdevice was placed and fixed in the microscope and the images were acquired by using objective lens of 10 and 20 X. The stage of the microscope allowed us to move and adjust the device for interrogation of the region of interest. Images of the flowing cells were captured by the high-speed camera at a frame rate of 2,000 frames/s and a shutter speed of 1/50,000 s. All the experimental assays for cells separation were performed at room temperature ($T = 22 \pm 2$ °C).

The flow rate of the working fluids through the microchannel was kept constant, at 100 µL/min, by means of a syringe pump (PHD Ultra, Harvard Apparatus, USA) fitted with a 5 mL syringe (Terumo, Japan). Inlet and outlet connections were performed by tubing. As the blood samples flowed within the microfluidic device, the cells were collected at the nine outlets into different reservoirs in order to evaluate the cell separation. The outlet orifices were made with a 1.5 mm diameter biopsy punch and connected to the reservoirs (Eppendorf) by tygon tubes.

To quantify the concentration of cells (WBCs and RBCs) in the source sample and at each outlet, an automatic hematology analyzer system (Sysmex XT-4000i) was used. This clinical equipment relies on fluorescent flow cytometry and hydrodynamic focusing technologies to allow the reliable identification and counting of cells. For each outlet, three samples of 150 µL were collected in order to perform the measurements three times and evaluate their reproducibility. The cell concentration (E_x) defined by Eq. (1) was quantified as the ratio between the number of cells of a given type (x) captured at the outlet (N_{out_x}) over the total number of the same type of cells in the source blood (N_{in_x}). Three types of cells were considered with subscript x referring to RBCs, WBCs and M (RBCs plus WBCs).

$$E_x = \left(\frac{N_{out\_x}}{N_{in\_x}}\right) \times 100\% \quad (1)$$

2.5. Image analysis

The image sequences recorded during the flow visualizations were analyzed and processed using the image processing tools from the software ImageJ (1.46r, NIH, USA) [47]. Several steps of pre-processing and image segmentation were performed in order to obtain well defined cell shapes. Briefly, in order to reduce static artifacts, an average background image was created from the original stack images, by averaging each pixel over the sequence of static images while using the ImageJ function Z project [46,48], and then subtracted from the individual stack images, so that at the end only the RBCs of interest remain. Brightness/Contrast adjustment was also applied to enhance the image quality, and the greyscale images were converted to binary images adjusting the threshold level. For that purpose, the Otsu threshold

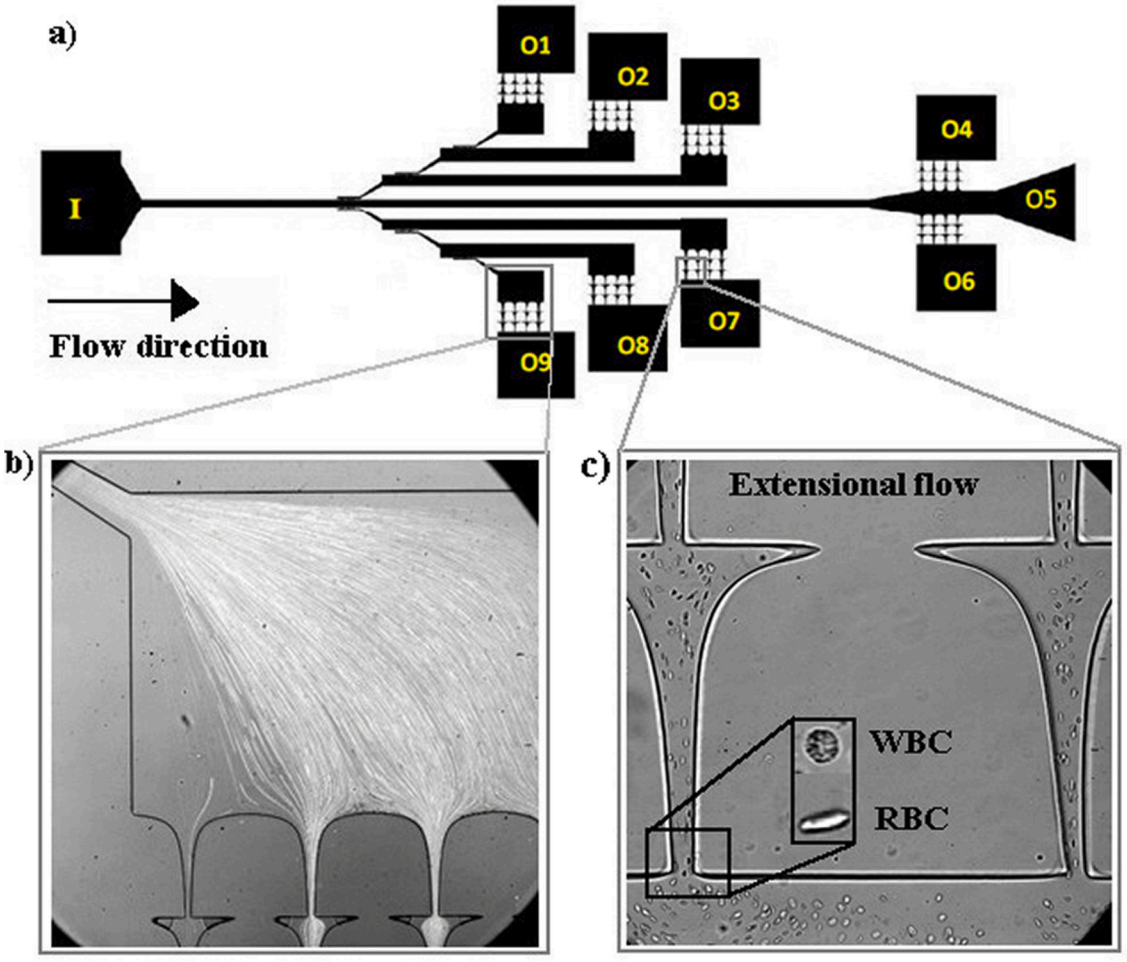

Fig. 2. a) Schematic representation and numeration of the microchannel outlets (O1 to O9); b) microscope image of the flow at the Outlet 9 and c) RBCs and WBCs under extensional flow at the Outlet 7.

method [49] was applied and, when required, the level was manually adjusted, resulting in well defined cells as black ellipsoidal objects against a white background. At the end, the flowing cells in the binary images were manually measured frame by frame with the wand tool function in ImageJ. The main output results of these measurements were the major and minor axis length of each individual cell (WBC and RBC from healthy and diabetic donors' blood) and the x-y coordinates of their centroids. More details about the image processing steps can be found in [4,46,50]. The deformation indexes (*DI*) of the samples were then calculated using

$$DI = \frac{L_{major} - L_{minor}}{L_{major} + L_{minor}}, \quad (2)$$

where L_{major} and L_{minor} refer to the lengths of the major and minor axis of the blood cell, respectively. Finally, the MTrackJ plugin from ImageJ was also used to assess the velocities and trajectories of the cells [51].

3. Results and discussion

3.1. Whole blood and working fluids rheology

Steady shear tests with healthy and pathological blood samples were performed at 37 and 22 °C. The samples hematocrit was standardized to 48% in order to minimize the influence of cell concentration. Diabetes mellitus type II is a disease characterized by elevated glucose in the blood circulation and it is generally accepted that blood viscosity is increased as a result of the disease [33]. Although the relation between blood glucose, diabetes and blood viscosity is still not completely understood, several works have demonstrated that patients with high levels of blood glucose have higher plasma viscosity, higher RBCs rigidity and higher aggregation [28,33,52]. Fig. 4a) and b) shows a comparison between the viscosity measured for both pathological and healthy blood samples, as a function of the shear rate. The whole blood viscosity (WBV) of diabetic patients is higher for all the tested shear rates, in line with experiments performed by Kostova et al. [33]. At low shear rates, the blood viscosity is strongly dependent on the RBCs aggregation while at high shear rates, the aggregated structures tend to breakdown and cells tend to elongate and align with the flow, being influenced by cells deformability. Pathological cells are less deformable and, consequently, will increase the blood viscosity.

By analyzing the viscosity at a single shear rate, it is clearly observed that the pathological WBV shows higher values. For example, at a shear rate of 25 s^{-1}, the mean WBV for pathological and healthy blood is 0.0118 Pa.s and 0.0096 Pa.s, respectively, at a temperature of 22 °C. In the same way, for a higher shear rate of 520 s^{-1}, the WBV presents values of 0.0079 Pa.s for pathological blood and 0.00565 Pa.s for healthy blood samples.

Regarding the working fluids (5 and 20% of Hct in Dx 40) used for the separation and deformability tests, their viscosity curves at T = 22 °C are shown in Fig. 4c) and d). Despite blood dilution in Dx 40, a higher viscosity at low shear rates is still observed for all samples especially at the hematocrit of 20% (Fig. 4d)). This high viscosity at low shear rates can now be related to both cell aggregation and the reduced cells

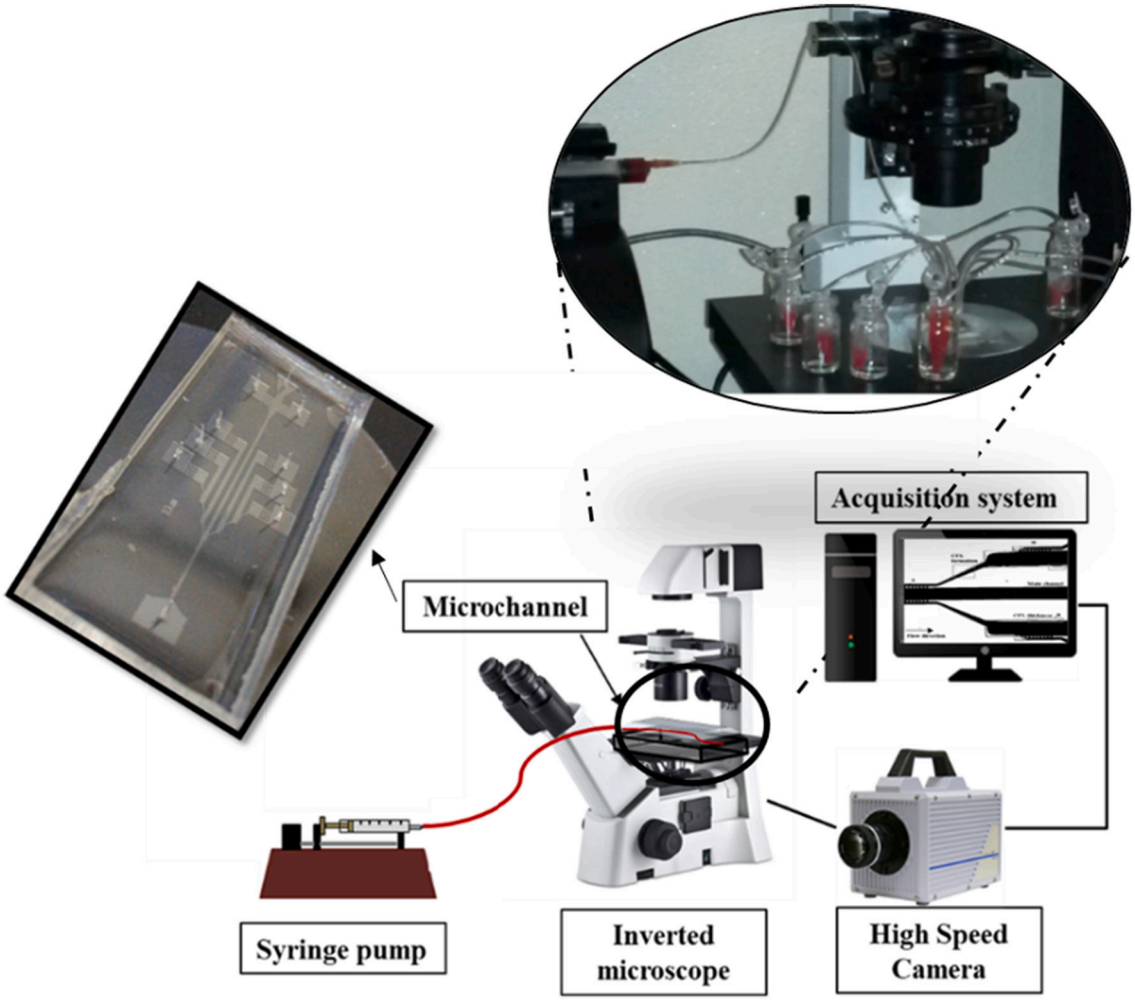

Fig. 3. Schematic representation of the experimental setup, comprising an inverted microscope coupled with a syringe pump system and a high-speed camera acquisition system.

deformability. Therefore, the separation and deformability assays will be an essential step for the characterization of the fluid and to obtain more detailed insights about the blood rheological properties and correlate them with the results of individual cell behavior.

3.2. Cell separation phenomena at the multi-step device

The cell separation and deformability experiments were performed at the same flow conditions without observing significant sedimentation, clogging, jamming or leakage problems that are likely to arise at microfluidic devices with multiple filters and bifurcations (see Fig. 5). The Reynolds number, based on the viscosity of the carrier fluid (5.2 mPa.s for Dx 40) and the hydraulic diameter, was below 1 at the smallest microchannel. Additionally, velocities obtained in this device for the dextran suspensions, to be presented in sub-section 3.4, are of the same order as the velocities observed in *in vivo* microvessels having diameters ranging from 80 to 500 μm [26].

The proposed multi-step microfluidic device comprises a sequence of cross-flow filters that plays a major role in the separation of cells based on their size. Besides the hydrodynamic mechanisms, it is well known that the combination of RBCs deformability and high wall shear rates promotes RBCs migration to the center of the microchannel. Also, the cells interaction and the margination process lead some WBCs toward the microchannel wall [53,54]. Thus, smaller WBCs and some deformable RBCs, when flowing near the pillars, tend to pass through the cross-flow filter barrier into the branch channels. Yet, when cells reach an asymmetric bifurcation, according to the bifurcation law, they tend to prefer the daughter channel with the higher flow rate [1,20]. The smaller dimensions of the branch channels, complemented with the cross-flow filters, help to create differences in the local flow rates. The combination of both effects can be seen in Fig. 5, where the local flow rate in the main channel is ~75.6 μL/min and at the daughter channels the smaller mean flow rate is ~20.6 μL/min.

Fig. 5 shows the combination of several hydrodynamics effects taking place inside the microdevice, as well as flow pattern variations over the various obstacle arrays in zones A, B and C (see Fig. 1). The CFL developed in the straight channel grows in size, not only downstream, but also when this fluid has the chance to flow laterally through the filter on the side wall, subsequently flowing through constrictions-expansions. In fact, it can be seen in Fig. 6a), b) and c), that the blood fraction passing through the successive divergent branches leads to an increase of the CFL thickness and, as a result, the amount of cells that are able to move to the next daughter channel is reduced. Hence, by combining all the hydrodynamics phenomena, it is possible not only to obtain a low concentration of cells at the outermost outlets (Fig. 6d)), but also to measure accurately the cell deformability of each individual cell.

3.3. Microdevice cell separation

The counting of WBCs and RBCs was performed off-chip, using an automated hematology system. By taking into account the values

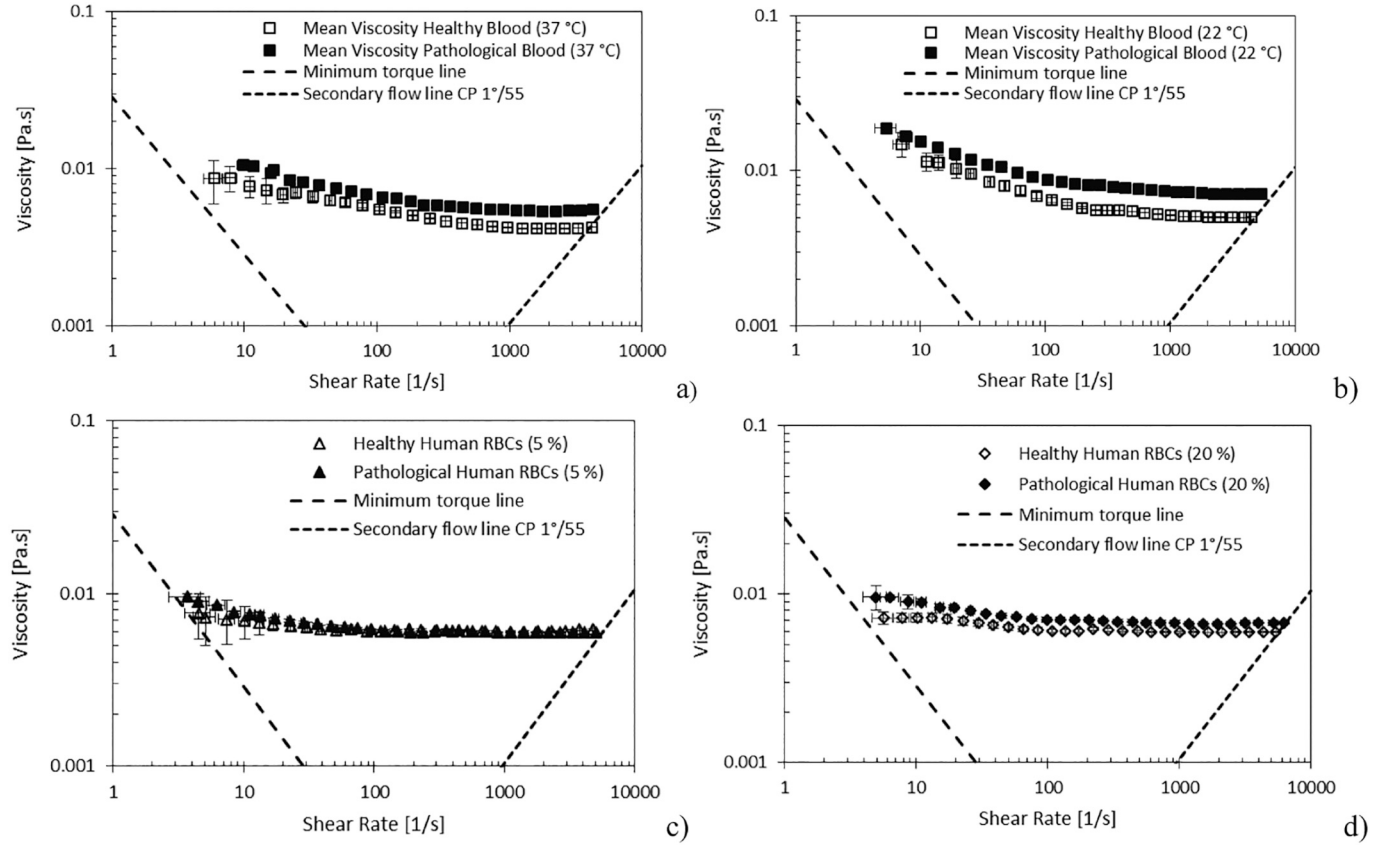

Fig. 4. Mean WBV for the patients with diabetes type II ($n = 15$) and for the control group of healthy individuals ($n = 5$) at: a) 22 °C and b) 37 °C. Viscosity curves of diluted blood in dextran 40 at: c) 5% and d) 20% of Hct obtained at 22 °C. Error bars represent the mean standard deviation at 95%.

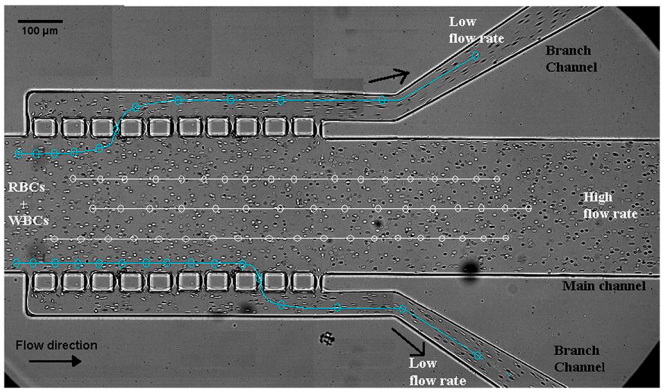

Fig. 5. Microscope image (20× objective) at zone A (see Fig. 1) of the microdevice. The lines with symbols represent schematically expected trajectories of different blood cells flowing through the main and branch microchannels.

obtained at the hematology system, it was possible to estimate the cells concentration, by considering the difference between the cells collected at the outlets and inlet. Table 1 lists the concentration of cells at the outlet of the experimental assays performed for the healthy donors ($n = 5$). The cell counting was performed three times for each sample.

The lowest concentrations were obtained through outlets O1 and O9, regardless of hematocrit, but for 5% Hct it was possible to get almost pure plasma, with a very low concentration of all cells (less or equal to 1%). For 20% Hct, the device was still able to achieve a good separation and the cell concentration at those outlets was E_M=3.58% (*cf.* Table 1). For both dilutions, around 44% of cells exited through outlets O4, O5 and O6. The cells that pass through the first cross-flow filters to the branch channels encounter the second pillar array and the majority of them are oriented to outlets O3 and O7, where the cell concentration was about 16 and 18%, for 5 and 20% Hct, respectively. For the outlets with two levels of pillar-array filtration (O2 and O8), the cells concentration can reach mean values of 10% and 7%, for 5 and 20% Hct, respectively. Overall, the sequence of cross-flow filters combined with the hydrodynamic effects allowed a gradual increment of the cell separation, where the lowest cell concentration was found at the outermost outlets (O1 and O9).

The results of cell separation with pathological blood from diabetic II patients are listed in Table 2. The results are qualitatively similar to those of healthy cells. However, quantitatively, they exhibit minor differences between the outlets of the device. The outlets located at the end of the main channel (O4, O5 and O6) have the highest total cell concentration, in the same way as for healthy cells flow separation, but outlet O5 has far less cells (19% to 21% against 32% to 35% for healthy cells). The outermost outlets O1 and O9 exhibit the lowest concentrations of the device, at around 4% and 6% of cells for 5% and 20% Hct, but pure plasma separation was not achieved as occurred with healthy cells (concentration at or below 1%).

In the flow tests performed with the 5% Hct of pathological blood samples, residual formation of agglomerates was observed at the cross-flow filters, whereas considerable agglomerates were observed at 20% Hct. This aggregation of pathological RBCs could be the result of their lower ability to deform, leading to their higher tendency to form large cell agglomerates that partially block the array gaps. However, after some time, the agglomerates tend to disaggregate due to the high local fluid velocities. In order to minimize these effects, each experiment was limited to a maximum time of 30 min, and in the initial 20 min we could not observe any cell agglomeration.

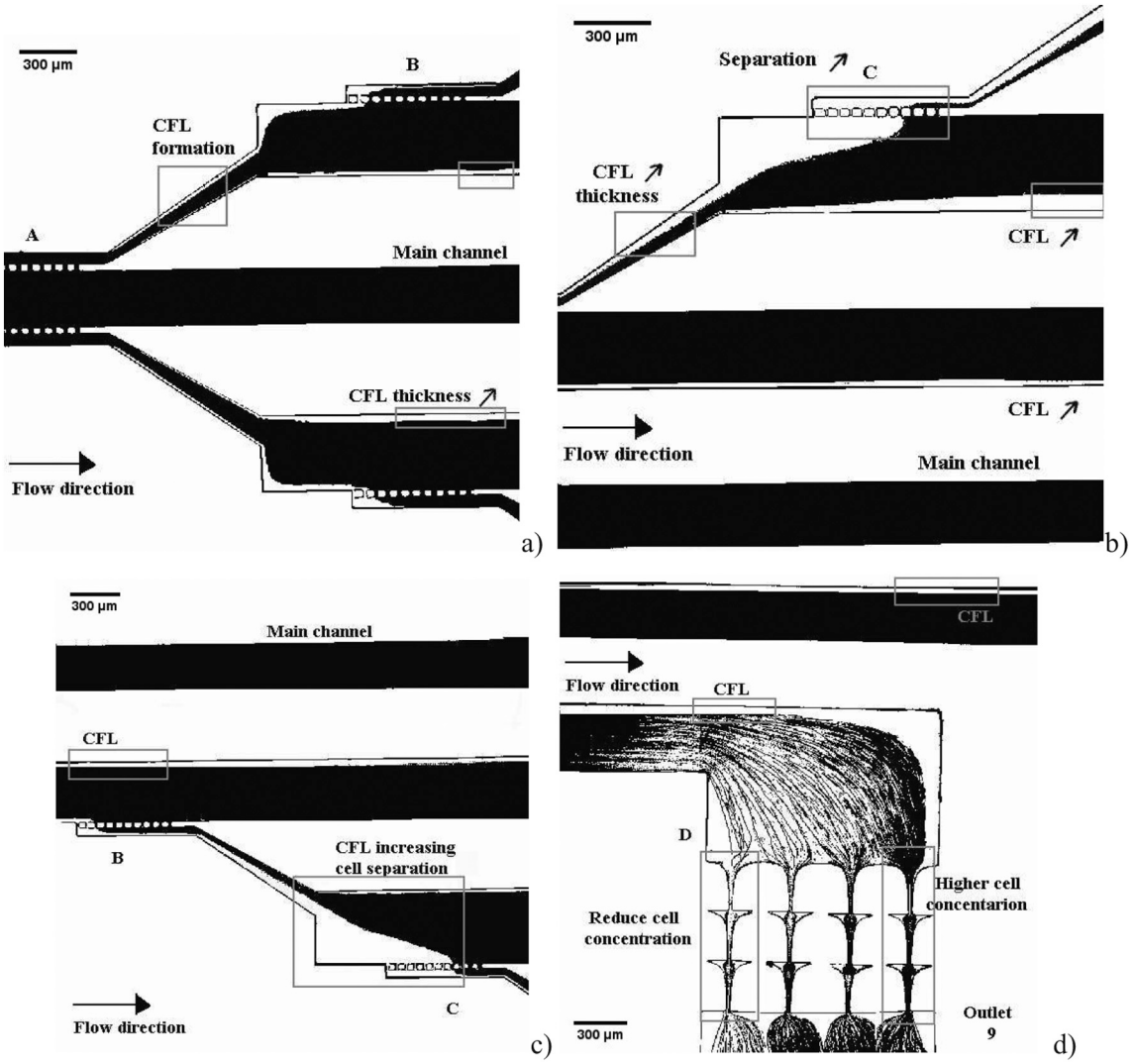

Fig. 6. Threshold microscopic images (10× objective) of the microchannel: a) zone A; b) zone C; c) zones B and C and d) zone D of the Outlet 9, for the flow visualizations, at 20% Hct.

Table 1
Microdevice cell concentration at each outlet for healthy blood dilution (5 and 20% Hct) and the standard deviation at 95% for $n = 5$.

Microdevice Outlets	Healthy blood at 5% Hct				Healthy blood at 20% Hct			
	E_{RBCs} (%)	E_{WBCs} (%)	E_M (%)	SD (95%)	E_{RBCs} (%)	E_{WBCs} (%)	E_M (%)	SD (95%)
O1	1.00	0.82	1.00	0.04	3.59	1.13	3.58	0.19
O2	11.67	9.79	11.67	1.41	5.64	5.36	5.64	0.30
O3	14.30	16.15	14.31	1.94	19.83	23.00	19.84	1.27
O4	5.14	4.40	5.14	0.91	5.64	4.85	5.64	0.62
O5	32.25	35.07	32.25	1.94	31.28	30.64	31.27	2.04
O6	7.15	5.06	7.15	1.65	5.33	4.88	5.33	0.84
O7	18.44	19.58	18.45	0.88	16.14	19.15	16.15	1.48
O8	9.28	8.65	9.28	1.14	8.97	9.30	8.97	0.36
O9	0.75	0.49	0.75	0.05	3.59	1.69	3.58	0.72

3.4. Deformability and cell velocity

The aim of the proposed microfluidic device is, not only to separate blood cells from the plasma, but also to measure the deformability of RBCs and WBCs at the hyperbolic contractions located upstream the outlets. Variations in blood cell deformability have been associated with several human diseases and, for the particular case of diabetes, the possible genetic and molecular causes for cell deformability alteration are still unclear. Hence, it is necessary to better understand this correlation. Fig. 7 shows cell deformability results at all outlets (60 cells per outlet) with hyperbolic geometries (15 cells per hyperbolic contraction), together with the corresponding centerline cell velocities, which were measured by tracking the RBCs and WBCs. The image sequences used to obtain the *DI* measurements were recorded during the flow of healthy and pathological blood with a 20% Hct. Most of the fluid exited through outlet O5, which has no hyperbolic contraction, while a low amount of cells cross the pillar barrier and the cell deformability can be analyzed. Note that cells flowing close to the walls, cells exhibiting

Table 2
Microchannel cell concentration, in each outlet for diabetic blood dilution (5 and 20% Hct) with standard deviation at 95% for $n = 15$.

Microdevice Outlets	Blood of diabetic patients at 5% Hct				Blood of diabetic patients at 20% Hct			
	E_{RBCs} (%)	E_{WBCs} (%)	E_M (%)	SD (95%)	E_{RBCs} (%)	E_{WBCs} (%)	E_M (%)	SD (95%)
O1	5.05	7.27	5.05	0.62	6.02	3.37	6.01	0.19
O2	12.63	12.73	12.63	0.87	10.65	13.20	10.63	0.30
O3	14.14	14.55	14.14	0.81	12.50	15.73	12.48	1.21
O4	11.11	12.36	11.11	0.54	7.87	8.71	7.86	0.62
O5	18.69	17.09	18.68	0.30	21.30	16.29	21.26	1.67
O6	11.11	9.09	11.11	0.54	10.65	10.39	10.63	0.84
O7	12.12	13.09	12.12	0.90	12.50	14.33	12.48	1.31
O8	11.11	10.18	11.10	0.10	12.04	13.76	12.02	0.36
O9	4.04	3.64	4.05	0.92	6.48	4.21	6.47	0.30

rotational motion upstream the hyperbolic contraction or rotating along the middle of the contraction were not measured (see Supplementary Video S1).

The velocity data demonstrate near symmetry between the up-down outlets, as expected due the device design, showing that the flow experiments were in equilibrium, Fig. 7a) and b). This equilibrium is extremely important to perform accurate comparison of the cells deformability. In addition, the velocities measured at the tested hyperbolic microchannel outlets are similar to those found in *in vivo* microvessels [26], therefore, this microdevice is able to deform cells similarly to what happens in *in vivo* environments.

The *DI* results show a significant difference between the behavior of healthy and pathological RBCs, with the deformability of the latter being 25% less that of the former (and relative to healthy RBCs), therefore confirming the correlation between the loss of RBCs deformability and the pathological condition. Specifically, the healthy RBCs reach peak *DI* values of 0.51 ± 0.01 at O3 and of 0.49 ± 0.02 at O7 (mean shear rate of 1609.33 s^{-1}), which corresponds to the two outlets with highest velocities, *cf.* Fig. 7a). For the outlets with lower velocities, O1, O4, O6 and O9, we measured lower *DI* values for the healthy RBCs, around 0.44 ± 0.02. On the other hand, the RBCs from diabetic type II blood samples have a mean *DI* of 0.3 ± 0.01 and, even at the outlets with higher velocities, their deformability does not have a significant increase, demonstrating that these cells are more rigid, therefore less able to elongate with the applied normal stress.

In contrast, the differences between healthy and pathological WBCs

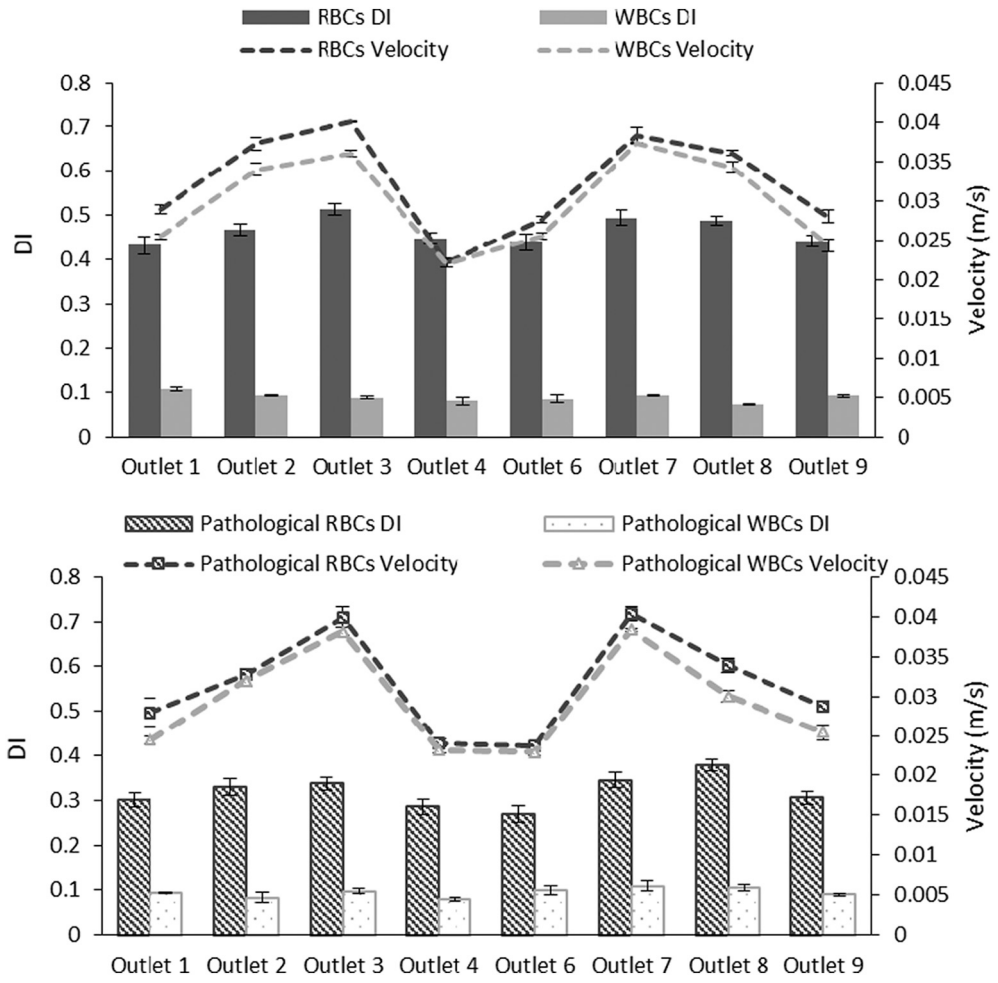

Fig. 7. Deformation index (*DI*) (a.u.) measurements at each outlet (total of 60 cells) and corresponding velocity (m/s) for the RBCs and WBCs with 20% Hct: a) healthy and b) pathological blood.

are negligible. The WBCs submitted to the same strong extensional flow and high shear rates as the RBCs reach a maximum *DI* of 0.11 (Outlets 3 and 7), corresponding to a mean shear rate of 1521 s^{-1}, ($\dot{\gamma} = U/Dh$). In addition, the deformability measurements showed WBCs flow trajectories taking place close to the walls of the hyperbolic geometries, subject to rotational motion (see Supplementary Video S1). The WBCs cytoskeleton structure, internal composition and their *in vivo* function are the main reasons for the rolling and arrest phenomena, allowing their capture from the blood flow to the endothelial cells. This flow behavior is one of the reasons why WBCs have consistently lower velocities than RBCs, as shown in Fig. 7. Note that the deformation of WBCs is usually a consequence of immune system activity [26]. Here, the deformability results reveal that, under the applied *in vitro* conditions, WBCs behaved as non-deformable cells due to the absence of immune activation even though there is a blood disease, here diabetes, that affects RBCs.

4. Conclusions

In the present study, a novel microfluidic device for cell separation and deformability assessment of RBCs and WBCs from blood samples was designed and fabricated. The main goal was to obtain a microfluidic system that works efficiently with microcirculation hematocrit values (~20%), under both healthy and pathological conditions. Hence, blood from healthy donors and from diabetes type II patients was used to perform the experimental separation and deformability assays.

For each blood sample the viscosity curves were initially obtained and discussed. The viscosity data showed that the pathological blood has always a higher viscosity than the healthy blood samples within the tested shear rates. These results are in good agreement with the literature and confirm that blood viscosity tends to increase in diabetic patients. Variations in blood viscosity and cell deformability have been associated with the diabetes disease, improving the possibility of microvascular complications. Appropriate RBCs flexibility is required to prevent disturbance to the blood flow in the microcirculation and to prevent occlusion episodes.

The developed multi-step microfluidic device was able to achieve a considerable cell reduction through the cross-flow filtration zones, which was essential to perform a correct deformability analysis at the device outlets. The measurements performed at the hyperbolic contractions have shown that the RBCs from the diabetic blood samples have deformability values about 25% lower when compared with those of healthy cells. In contrast, WBCs presented low and similar deformability indices regardless of whether they belong to healthy or pathological blood.

The proposed multi-step microfluidic device may have the potential to become a new promise strategy for innumerable applications in clinical diagnosis and biomedical research. Particularly, such microdevice could be part of an integrated blood-on-a-chip system to improve the separation efficiency of different blood cells from unprocessed whole blood, benefiting from the small sample volumes, as well as being economically accessible, allowing accurate and simple single-cell assays.

Supplementary data to this article can be found online at https://doi.org/10.1016/j.mne.2022.100149.

Declaration of Competing Interest

The authors declare that they have no known competing financial interests or personal relationships that could have appeared to influence the work reported in this paper.

Acknowledgments

This work was supported by Projects NORTE-01-0145-FEDER-028178, NORTE-01-0145-FEDER-029394, NORTE-01-0145-FEDER-030171 funded by COMPETE2020, NORTE2020, PORTUGAL2020, and FEDER. This work was also supported by Fundação para a Ciência e a Tecnologia (FCT) under the strategic grants UIDB/04077/2020 and UIDB/00532/2020. D. Pinho and V. Faustino acknowledge the Ph.D. scholarships SFRH/BD/89077/2012 and SFRH/BD/99696/2014, respectively, both provided by FCT. Susana Catarino thanks FCT for her contract funding provided through 2020.00215.CEECIND. F. T. Pinho is thankful to FCT for financial support through projects LA/P/0045/2020 of the Associate Laboratory in Chemical Engineering (ALiCE) and projects UIDB/00532/2020 and UIDP/00532/2020 of Centro de Estudos de Fenómenos de Transporte.

References

[1] Z.T.F. Yu, K.M.A. Yong, J. Fu, Microfluidic blood cell preparation: now and beyond, Small. 10 (2014) 1687–1703, https://doi.org/10.1002/smll.201302907.
[2] J. Choi, J. Hyun, S. Yang, On-chip extraction of intracellular molecules in White blood cells from whole blood, Sci. Rep. 5 (2015) 15167, https://doi.org/10.1038/srep15167.
[3] S. Tripathi, Y.V.B. Kumar, A. Agrawal, A. Prabhakar, S.S. Joshi, Microdevice for plasma separation from whole human blood using bio-physical and geometrical effects, Sci. Rep. 6 (2016) 26749, https://doi.org/10.1038/srep26749.
[4] V. Faustino, R.O. Rodrigues, D. Pinho, E. Costa, A. Santos-Silva, V. Miranda, J. S. Amaral, R. Lima, A microfluidic deformability assessment of pathological red blood cells flowing in a hyperbolic converging microchannel, Micromachines. 10 (2019), https://doi.org/10.3390/mi10100645.
[5] A.A.S. Bhagat, H. Bow, H.W. Hou, S.J. Tan, J. Han, C.T. Lim, Microfluidics for cell separation, Med. Biol. Eng. Comput. 48 (2010) 999–1014, https://doi.org/10.1007/s11517-010-0611-4.
[6] H.W. Hou, A.A.S. Bhagat, A.G.L. Chong, P. Mao, K.S.W. Tan, J. Han, C.T. Lim, Deformability based cell margination—a simple microfluidic design for malaria-infected erythrocyte separation, Lab Chip 10 (2010) 2605–2613, https://doi.org/10.1039/c003873c.
[7] H.W. Hou, A.A.S. Bhagat, W.C. Lee, S. Huang, J. Han, C.T. Lim, Microfluidic devices for blood fractionation, Micromachines. 2 (2011) 319–343, https://doi.org/10.3390/mi2030319.
[8] N.F. Zeng, J.E. Mancuso, A.M. Zivkovic, J.T. Smilowitz, W.D. Ristenpart, Red blood cells from individuals with abdominal obesity or metabolic abnormalities exhibit less deformability upon entering a constriction, PLoS One 11 (2016), https://doi.org/10.1371/journal.pone.0156070.
[9] X.H. Liu, X. Wang, The deformation of an adherent leukocyte under steady shear flow: a numerical study, J. Biomech. 37 (2004) 1079–1085, https://doi.org/10.1016/j.jbiomech.2003.11.015.
[10] M.J. Rosenbluth, W.A. Lam, D.A. Fletcher, Analyzing cell mechanics in hematologic diseases with microfluidic biophysical flow cytometry, Lab Chip 8 (2008) 1062–1070, https://doi.org/10.1039/b802931h.
[11] A. Sabo, V. Jakovljević, M. Stanulović, L. Lepsanović, D. Pejin, Red blood cell deformability in diabetes mellitus: effect of phytomenadione, Int. J. Clin. Pharmacol. Ther. Toxicol. 31 (1993) 1–5. http://europepmc.org/abstract/MED/8444511.
[12] R. Suwanarusk, B.M. Cooke, A.M. Dondorp, K. Silamut, J. Sattabongkot, N. J. White, R. Udomsangpetch, The deformability of red blood cells parasitized by plasmodium falciparum and P. vivax, J. Infect. Dis. 189 (2004) 190–194, https://doi.org/10.1086/380468.
[13] Y.T. Yaylali, I. Susam, E. Demir, M. Bor-Kucukatay, B. Uludag, E. Kilic-Toprak, G. Erken, D. Dursunoglu, Increased red blood cell deformability and decreased aggregation as potential adaptive mechanisms in the slow coronary flow phenomenon, Coron. Artery Dis. 24 (2013) 11–15, https://doi.org/10.1097/MCA.0b013e32835b0bdf.
[14] G. Tomaiuolo, Biomechanical properties of red blood cells in health and disease towards microfluidics, Biomicrofluidics. 8 (2014) 51501, https://doi.org/10.1063/1.4895755.
[15] D. Pinho, V. Carvalho, I.M. Gonçalves, S. Teixeira, R. Lima, Visualization and measurements of blood cells flowing in microfluidic systems and blood rheology: a personalized medicine perspective, J. Pers. Med. 10 (2020) 1–18, https://doi.org/10.3390/jpm10040249.
[16] M. Toner, D. Irimia, Blood-on-a-chip, Annu. Rev. Biomed. Eng. 7 (2005) 77–103, https://doi.org/10.1146/annurev.bioeng.7.011205.135108.
[17] S.O. Catarino, R.O. Rodrigues, D. Pinho, J.M. Miranda, G. Minas, R. Lima, Blood cells separation and sorting techniques of passive microfluidic devices: from fabrication to applications, Micromachines. 10 (2019), https://doi.org/10.3390/mi10090593.
[18] X. Chen, D. Cui, C. Liu, H. Li, Microfluidic chip for blood cell separation and collection based on crossflow filtration, Sensors Actuators B Chem. 130 (2008) 216–221, https://doi.org/10.1016/j.snb.2007.07.126.
[19] B.E. Layton, B. Lynch, T. Peter, B. Jamieson, Red blood cell sorting with a multi-bed microfabricated filter, J. Micromech. Microeng. 22 (2012), https://doi.org/10.1088/0960-1317/22/2/025009.
[20] S. Yang, A. Ündar, J.D. Zahn, A microfluidic device for continuous, real time blood plasma separation, Lab Chip 6 (2006) 871–880, https://doi.org/10.1039/B516401J.
[21] K.-A. Hyun, K. Kwon, H. Han, S.-I. Kim, H.-I. Jung, Microfluidic flow fractionation device for label-free isolation of circulating tumor cells (CTCs) from breast cancer

patients, Biosens. Bioelectron. 40 (2013) 206–212, https://doi.org/10.1016/J.BIOS.2012.07.021.
[22] M.G. Lee, J.H. Shin, C.Y. Bae, S. Choi, J.K. Park, Label-free cancer cell separation from human whole blood using inertial microfluidics at low shear stress, Anal. Chem. 85 (2013) 6213–6218, https://doi.org/10.1021/ac4006149.
[23] A. Prabhakar, Y.V.B.V. Kumar, S. Tripathi, A. Agrawal, A novel, compact and efficient microchannel arrangement with multiple hydrodynamic effects for blood plasma separation, Microfluid. Nanofluid. 18 (2015) 995–1006, https://doi.org/10.1007/s10404-014-1488-6.
[24] S. Tripathi, Y.V.B.V. Kumar, A. Prabhakar, S.S. Joshi, A. Agrawal, Passive blood plasma separation at the microscale: a review of design principles and microdevices, J. Micromech. Microeng. 25 (2015), 083001, https://doi.org/10.1088/0960-1317/25/8/083001.
[25] P. Sethu, A. Sin, M. Toner, Microfluidic diffusive filter for apheresis (leukapheresis), Lab Chip 6 (2006) 83–89, https://doi.org/10.1039/B512049G.
[26] R.O. Rodrigues, D. Pinho, V. Faustino, R. Lima, A simple microfluidic device for the deformability assessment of blood cells in a continuous flow, Biomed. Microdevices 17 (2015) 108, https://doi.org/10.1007/s10544-015-0014-2.
[27] Y.I. Cho, M.P. Mooney, D.J. Cho, D.J. Mooney Mp Fau Cho, D.J. Cho, M.P. Mooney, D.J. Cho, Hemorheological disorders in diabetes mellitus, J. Diabetes Sci. Technol. 2 (2008) 1130–1138, https://doi.org/10.1177/193229680800200622.
[28] C. Irace, C. Carallo, F. Scavelli, M.S. De Franceschi, T. Esposito, A. Gnasso, Blood viscosity in subjects with normoglycemia and prediabetes, Diabetes Care 37 (2014) 488–492, https://doi.org/10.2337/dc13-1374.
[29] S. Shin, Y.-H. Ku, J.-X. Ho, Y.-K. Kim, J.-S. Suh, M. Singh, Progressive impairment of erythrocyte deformability as indicator of microangiopathy in type 2 diabetes mellitus, Clin. Hemorheol. Microcirc. 36 (2007) 253–261. http://content.iospress.com/articles/clinical-hemorheology-and-microcirculation/ch977.
[30] R. Agrawal, T. Smart, J. Nobre-Cardoso, C. Richards, R. Bhatnagar, A. Tufail, D. Shima, P.H. Jones, C. Pavesio, Assessment of red blood cell deformability in type 2 diabetes mellitus and diabetic retinopathy by dual optical tweezers stretching technique, Sci. Rep. 6 (2016) 15873, https://doi.org/10.1038/srep15873.
[31] B. Riquelme, P. Foresto, M. D'Arrigo, J. Valverde, R. Rasia, A dynamic and stationary rheological study of erythrocytes incubated in a glucose medium, J. Biochem. Biophys. Methods 62 (2005) 131–141, https://doi.org/10.1016/j.jbbm.2004.10.004.
[32] B. de Cindio, D. Gabriele, G. Catapano, P. Fata, R. Hackel, R. Bonofiglio, The blood rheology in renal pathology, Ann. Ist. Super. Sanita 43 (2007) 156–163.
[33] V. Kostova, N. Antonova, I. Velcheva, B. Ivanov, Comparative analysis of the rheological properties of blood in patients with type 2 diabetes, Ser. Biomech. 27 (2012) 80–85.
[34] L. Campo-Deaño, R.P.A. Dullens, D.G.A.L. Aarts, F.T. Pinho, M.S.N. Oliveira, Viscoelasticity of blood and viscoelastic blood analogues for use in polydymethylsiloxane in vitro models of the circulatory system, Biomicrofluidics. 7 (2013), https://doi.org/10.1063/1.4804649.
[35] P.C. Sousa, J. Carneiro, R. Vaz, A. Cerejo, F.T. Pinho, M.A. Alves, M.S.N. Oliveira, Shear viscosity and nonlinear behavior of whole blood under large amplitude oscillatory shear, Biorheology. 50 (2013) 269–282, https://doi.org/10.3233/BIR-130643.
[36] V. Faustino, S.O. Catarino, R. Lima, G. Minas, Biomedical microfluidic devices by using low-cost fabrication techniques: a review, J. Biomech. 49 (2016) 2280–2292, https://doi.org/10.1016/j.jbiomech.2015.11.031.
[37] V.C. Pinto, P.J. Sousa, V.F. Cardoso, G. Minas, Optimized SU-8 processing for low-cost microstructures fabrication without cleanroom facilities, Micromachines. 5 (2014) 738–755, https://doi.org/10.3390/mi5030738.
[38] D.F. James, G.M. Chandler, S.J. Armour, A converging channel rheometer for the measurement of extensional viscosity, J. Nonnewton. Fluid Mech. 35 (1990) 421–443, https://doi.org/10.1016/0377-0257(90)85063-5.
[39] V. Faustino, S.O. Catarino, D. Pinho, R. Lima, G. Minas, A passive microfluidic device based on crossflow filtration for cell separation measurements: a spectrophotometric characterization, Biosensors. 8 (2018) 125, https://doi.org/10.3390/bios8040125.
[40] R. Lima, T. Ishikawa, Y. Imai, T. Yamaguchi, Blood flow behavior in microchannels: past, current and future trends, in: A.A.M. Ricardo Dias Rui Lima, T.M. Mata (Eds.), Single Two-Phase Flows Chem. Biomed. Eng., Bentham science, 2012, pp. 513–547.
[41] M.M. Kersaudy-Kerhoas, E. Sollier, Micro-scale blood plasma separation: from acoustophoresis to egg-beaters, Lab Chip 13 (2013) 3323–3346, https://doi.org/10.1039/C3LC50432H.
[42] D.R. Gossett, W.M. Weaver, A.J. Mach, S.C. Hur, H.T.K. Tse, W. Lee, H. Amini, D. Di Carlo, Label-free cell separation and sorting in microfluidic systems, Anal. Bioanal. Chem. 397 (2010) 3249–3267, https://doi.org/10.1007/s00216-010-3721-9.
[43] S.S. Lee, Y. Yim, K.H. Ahn, S.J. Lee, Extensional flow-based assessment of red blood cell deformability using hyperbolic converging microchannel, Biomed. Microdevices 11 (2009) 1021–1027, https://doi.org/10.1007/s10544-009-9319-3.
[44] T. Yaginuma, M.S.N. Oliveira, R. Lima, T. Ishikawa, T. Yamaguchi, Human red blood cell behavior under homogeneous extensional flow in a hyperbolic-shaped microchannel, Biomicrofluidics. 7 (2013) 54110, https://doi.org/10.1063/1.4820414.
[45] R.O. Rodrigues, R. Lopes, D. Pinho, A.I. Pereira, V. Garcia, S. Gassmann, P. C. Sousa, R. Lima, In vitro blood flow and cell-free layer in hyperbolic microchannels: visualizations and measurements, BioChip J. 10 (2016) 9–15, https://doi.org/10.1007/s13206-016-0102-2.
[46] V. Faustino, D. Pinho, T. Yaginuma, R.C. Calhelha, I.C.F.R.I. Ferreira, R. Lima, Extensional flow-based microfluidic device: deformability assessment of red blood cells in contact with tumor cells, BioChip J. 8 (2014) 42–47, https://doi.org/10.1007/s13206-014-8107-1.
[47] M.D. Abramoff, P.J. Magalhães, S.J. Ram, Image Processing with ImageJ 11, 2022, pp. 36–42 (n.d.).
[48] P. Kelly, D. Karten, Zproject Plugin, 2022 (n.d.).
[49] S. Kim, R.L. Kong, A.S. Popel, M. Intaglietta, P.C. Johnson, A computer-based method for determination of the cell-free layer width in microcirculation, Microcirculation. 13 (2006) 199–207, https://doi.org/10.1080/10739680600556878.
[50] V. Faustino, D. Pinho, T. Yaginuma, R.C. Calhelha, G.M. Kim, S. Arana, I.C.F. R. Ferreira, M.S.N. Oliveira, R. Lima, Flow of Red Blood Cells Suspensions Through Hyperbolic Microcontractions, 2014, https://doi.org/10.1007/978-94-007-7769-9_9.
[51] E. Meijering, I. Smal, G. Danuser, Tracking in molecular bioimaging, Signal Process. Mag. IEEE. 23 (2006) 46–53, https://doi.org/10.1109/MSP.2006.1628877.
[52] Y. Deng, D.P. Papageorgiou, X. Li, N. Perakakis, C.S. Mantzoros, M. Dao, G. E. Karniadakis, Quantifying fibrinogen-dependent aggregation of red blood cells in type 2 diabetes mellitus, Biophys. J. 119 (2020) 900–912, https://doi.org/10.1016/j.bpj.2020.07.026.
[53] A. Yazdani, X. Li, G.E. Karniadakis, Dynamic and rheological properties of soft biological cell suspensions, Rheol. Acta 55 (2016) 433–449, https://doi.org/10.1007/s00397-015-0869-4.
[54] K.H.K. Wong, J.M. Chan, R.D. Kamm, J. Tien, Microfluidic models of vascular functions, Annu. Rev. Biomed. Eng. 14 (2012) 205–230, https://doi.org/10.1146/annurev-bioeng-071811-150052.